

Metaphyseal Dysplasia with Maxillary Hypoplasia and Brachydactyly Is Caused by a Duplication in *RUNX2*

Pierre Moffatt,^{1,2,7} Mouna Ben Amor,^{1,7} Francis H. Glorieux,^{1,2} Paul Roschger,³ Klaus Klaushofer,³ Jeremy A. Schwartzentruber,⁴ Andrew D. Paterson,⁵ Pingzhao Hu,⁵ Christian Marshall,⁵ FORGE Canada Consortium,⁸ Somayyeh Fahiminiya,² Jacek Majewski,² Chandree L. Beaulieu,⁶ Kym M. Boycott,⁶ and Frank Rauch^{1,2,*}

Metaphyseal dysplasia with maxillary hypoplasia and brachydactyly (MDMHB) is an autosomal-dominant bone dysplasia characterized by metaphyseal flaring of long bones, enlargement of the medial halves of the clavicles, maxillary hypoplasia, variable brachydactyly, and dystrophic teeth. We performed genome-wide SNP genotyping in five affected and four unaffected members of an extended family with MDMHB. Analysis for copy-number variations revealed that a 105 kb duplication within *RUNX2* segregated with the MDMHB phenotype in a region with maximum linkage. Real-time PCR for copy-number variation in genomic DNA in eight samples, as well as sequence analysis of fibroblast cDNA from one subject with MDMHB confirmed that affected family members were heterozygous for the presence of an intragenic duplication encompassing exons 3 to 5 of *RUNX2*. These three exons code for the Q/A domain and the functionally essential DNA-binding runt domain of *RUNX2*. Transfection studies with murine *Runx2* cDNA showed that cellular levels of mutated *RUNX2* were markedly higher than those of wild-type *RUNX2*, suggesting that the *RUNX2* duplication found in individuals with MDMHB leads to a gain of function. Until now, only loss-of-function mutations have been detected in *RUNX2*; the present report associates an apparent gain-of-function alteration of *RUNX2* function with a distinct rare disease.

Metaphyseal dysplasia with maxillary hypoplasia and brachydactyly (MDMHB [MIM 156510]) is an autosomal-dominant bone dysplasia first described by Halal et al. in 1982 in a French Canadian family from the Gaspésie region in Quebec.¹ Affected family members had metaphyseal flare and thin diaphyseal cortices of long bones, bilateral shortness of middle phalanges or metacarpals, and maxillary hypoplasia. Other skeletal anomalies included mild short stature, enlargement of the medial halves of the clavicles, wide ischial and pubic bones, mild thickening of frontal and parietal skull bones, platyspondyly, and a general radiographic impression of osteoporosis, even though bone density measurements were not reported. Teeth were yellowish and dystrophic, leading to total dental extraction before the end of the second decade in the majority of affected individuals. No extra-skeletal abnormalities were noted. It appears that no further MDMHB cases have been reported since this initial description.

We have identified six individuals from a kindred whose clinical and radiographic phenotype closely resembles that of the subjects described by Halal et al.¹ and who also originate from the Gaspésie region in Quebec (Figure 1; Tables S1 and S2 available online). Histomorphometric

analysis of transiliac bone biopsy samples (from subjects IV-1, IV-2, and IV-6) showed thin cortices and a low amount of trabecular bone (Figure 1K). Mineral apposition rate, a marker of bone formation, was low, suggesting a defect in osteoblast function, whereas osteoclast surface, a marker of bone resorption, was normal (Figure 1L). Biochemical parameters of bone and mineral metabolism were mostly within normal limits (Table S3). Lumbar spine bone mineral density was low (z score < -2) for three subjects but was within normal limits for the others. However, peripheral quantitative computed tomography of the radius showed that cortices were very thin at both the metaphysis and the diaphysis (Table S3).

To search for the disease-causing mutation in this family, we obtained DNA from five affected and four unaffected family members (Figure 1A). With approval from the Institutional Review Board of McGill University, we obtained informed consent; assent was obtained from participants aged less than 18 years. We performed whole-genome SNP genotyping in all nine individuals with the Human Omni2.5-Quad chip (Illumina, San Diego, CA). MERLIN software (version 1.1.2) was used for parametric linkage analysis after pruning for linkage disequilibrium.² The maximum achievable LOD score of

¹Genetics Unit, Shriners Hospital for Children, Montréal, QC H3G 1A6, Canada; ²Department of Human Genetics, McGill University, Montréal, QC H3A 1B1, Canada; ³Ludwig Boltzmann Institute of Osteology at the Hanusch Hospital of WGKK and AUA Trauma Center Meidling, 1st Med. Department, Hanusch Hospital, Vienna 1140, Austria; ⁴McGill University and Genome Québec Innovation Centre, Montréal, QC H3A 0G1, Canada; ⁵Program in Genetics and Genome Biology, The Center for Applied Genomics, The Hospital for Sick Children Research Institute, and Dalla Lana School of Public Health, University of Toronto, Toronto, ON M5G 1L7, Canada; ⁶Children's Hospital of Eastern Ontario Research Institute, University of Ottawa, Ottawa, ON K1H 8L1, Canada

⁷These authors contributed equally to this work

⁸FORGE Steering Committee members are listed in the Acknowledgments

*Correspondence: frauch@shriners.mcgill.ca

<http://dx.doi.org/10.1016/j.ajhg.2012.12.001>. ©2013 by The American Society of Human Genetics. All rights reserved.

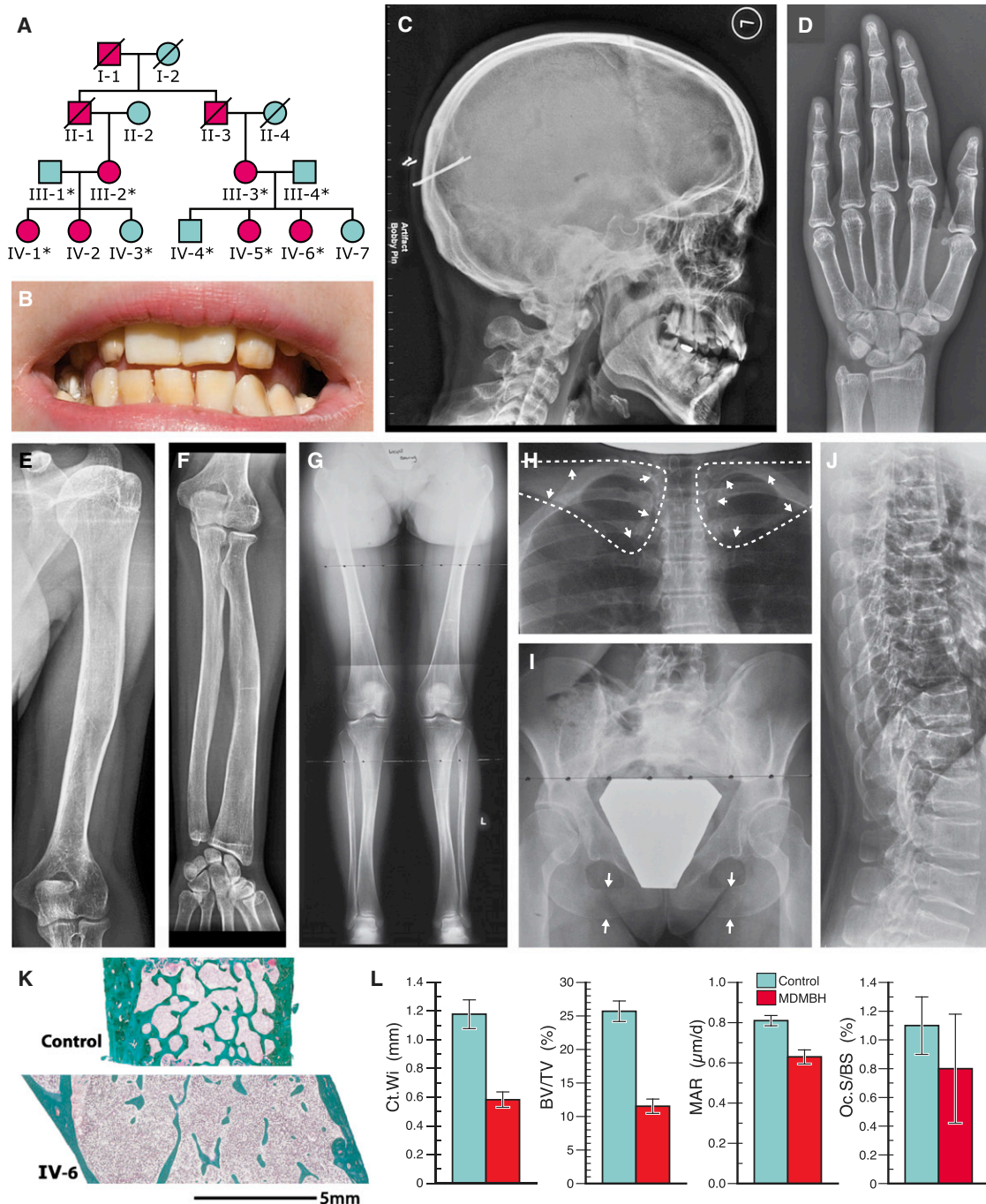


Figure 1. Clinical Information on a Family with MDMHB

(A) Pedigree. Individuals who contributed DNA for SNP genotyping are marked with an asterisk.

(B) Dental phenotype of subject IV-5 at 20 years of age, showing dysplastic and yellowish teeth.

(C–J) Radiographs of subject IV-5 at the age of 20 years, showing a thick cranial vault (C) as well as undermodeled metaphyses and thin cortices at hand and wrist (D), humerus (E), forearm (F), and lower extremities (G); enlarged medial portions of the clavicles (H, dashed lines surround the clavicles, the arrows show the precise location of the bone contour); widened symphyseal arches of the ischial (arrows) and pubic bones (I); and irregular shape and compression of vertebrae (J).

(K) Transiliac bone biopsy specimen from a control subject (top) and from subject IV-6 (bottom), both aged 17 years, showing enlarged bone size, thin cortices, and a low amount of trabecular bone in the sample from the affected individual.

(L) Histomorphometric results for samples from subjects IV-1, IV-2, and IV-6 and for age-matched controls ($n = 12$; from Glorieux et al.¹¹). Mean (error bars: SE) results for cortical width (Ct.Wi), trabecular bone volume per tissue volume (BV/TV), mineral apposition rate (MAR), and osteoclast-covered surface per bone surface (Oc.S/BS) are shown.

2.1 was obtained for regions on chromosomes 6, 11, and 15 (Table S4). Genomic DNA from subjects IV-1 and IV-5 was captured with the Agilent SureSelect 50 Mb

oligonucleotide library (Agilent Technologies Inc., Santa Clara, CA) and was sequenced with 100 paired-end reads on Illumina HiSeq2000. By using a bioinformatics

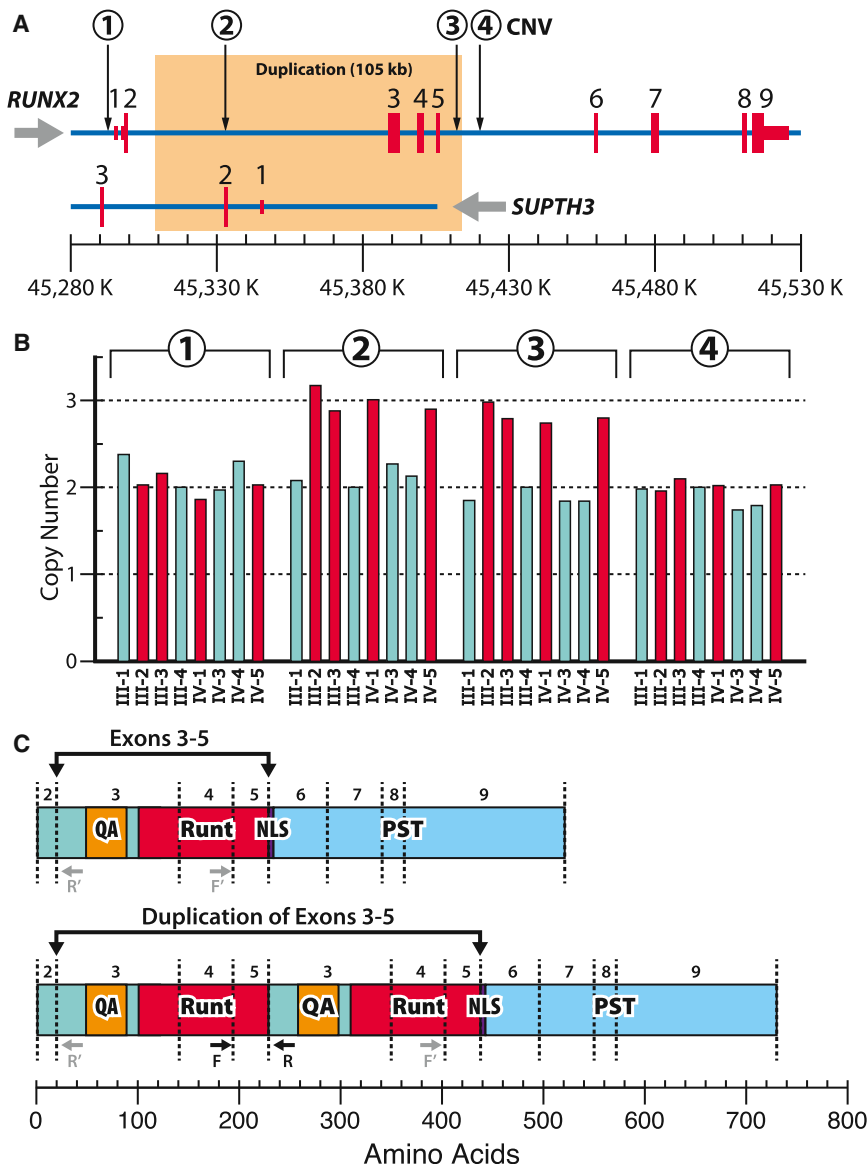


Figure 2. Duplication in *RUNX2*

(A) The genomic organization of the *RUNX2* locus on chromosome 6. The *RUNX2* gene has nine exons. The first two exons of *SUPT3H*, which is transcribed in the opposite direction (arrow), overlap with intron 2 of *RUNX2*. The locations analyzed by qPCR for copy number state are indicated by circled numbers.

(B) The qPCR analysis shows copy number state three for affected individuals III-2, III-3, IV-1, and IV-5 at locations 2 (Hs01529684_cn; location 45,332,959) and 3 (Hs04907414_cn; location 45,412,249), but copy number state two at locations 1 (Hs04922096_cn; location 45,292,671) and 4 (Hs06792104_cn; location 45,420,087). Unaffected individuals III-1, III-4, IV-3, and IV-4 have a copy number state two at all locations.

(C) Protein structure of wild-type *RUNX2* (top) and *RUNX2* with duplication of exons 3 to 5. The *RUNX2* domains are QA (poly Q/A repeat), Runt (runt domain), NLS (nuclear localization sequence), and PST (proline/serine/threonine-rich domain). The border positions of the corresponding exons are shown by the numbers and dotted vertical lines. The position of the primers used for PCR and sequencing of fibroblast cDNA of subject IV-6 is shown by arrows labeled F and R. Only cDNA carrying the duplication will result in a PCR product. No PCR amplification occurs when primers anneal to the unmutated cDNA (locations F' and R', in gray).

result in nonsense-mediated decay. We therefore judged it unlikely that the effect of the duplication on *SUPT3H* is involved in the pathogenesis of MDMHB and did not

investigate this gene further. In contrast, *RUNX2* codes for a transcription factor that is essential for bone formation.^{4,5} *RUNX2* haploinsufficiency leads to cleidocranial dysplasia (CCD [MIM 119600]).^{6,7} A duplication of exons 3 to 5 is predicted to lead to an in-frame addition to the *RUNX2* sequence. We therefore performed further investigations on *RUNX2*.

The duplication was confirmed by real-time PCR in genomic DNA from four affected and four unaffected family members (Figure 2B). All affected individuals had three copies for the two locations within the sequence affected by the duplication, but two copies at locations telomeric and centromeric of this region. Unaffected family members had two copies for all four locations. This confirmed the presence of a duplication that stretches from intron 2 to intron 5 of *RUNX2* and thus includes exons 3 to 5 of *RUNX2*. These three exons code for the Q/A domain and the runt domain of *RUNX2* (Figure 2C). The Q/A domain consists of a stretch of 23 glutamine residues

pipeline as previously described,³ we found that the 2 subjects shared 17 previously undescribed variants, none of which were located within any of the linkage regions. The SNP array data were analyzed for copy-number variations (CNV) with PennCNV, IPN, CNVpartition, and QuantiSNP algorithms. These CNV analyses showed that all affected individuals of the pedigree had a 105 kb duplication within the linked region on chromosome 6 (chromosomal location 6p12.3; physical position 6: 45,308,920–45,413,885; hg19) whereas this duplication was absent in all unaffected family members (Figure S1). Smaller duplications affecting intronic areas within this region have been reported in CNV databases.

The duplicated sequence contains exons 3 to 5 of *RUNX2* (MIM 600211, RefSeq accession number NM_001024630.3) and exons 1 and 2 of *SUPT3H* (MIM 602947) (Figure 2A). The function of *SUPT3H* (suppressor of Ty 3 homolog) is unknown. If the duplicated exons of *SUPT3H* are transcribed, they would lead to a frameshift and probably

investigate this gene further. In contrast, *RUNX2* codes for a transcription factor that is essential for bone formation.^{4,5} *RUNX2* haploinsufficiency leads to cleidocranial dysplasia (CCD [MIM 119600]).^{6,7} A duplication of exons 3 to 5 is predicted to lead to an in-frame addition to the *RUNX2* sequence. We therefore performed further investigations on *RUNX2*.

The duplication was confirmed by real-time PCR in genomic DNA from four affected and four unaffected family members (Figure 2B). All affected individuals had three copies for the two locations within the sequence affected by the duplication, but two copies at locations telomeric and centromeric of this region. Unaffected family members had two copies for all four locations. This confirmed the presence of a duplication that stretches from intron 2 to intron 5 of *RUNX2* and thus includes exons 3 to 5 of *RUNX2*. These three exons code for the Q/A domain and the runt domain of *RUNX2* (Figure 2C). The Q/A domain consists of a stretch of 23 glutamine residues

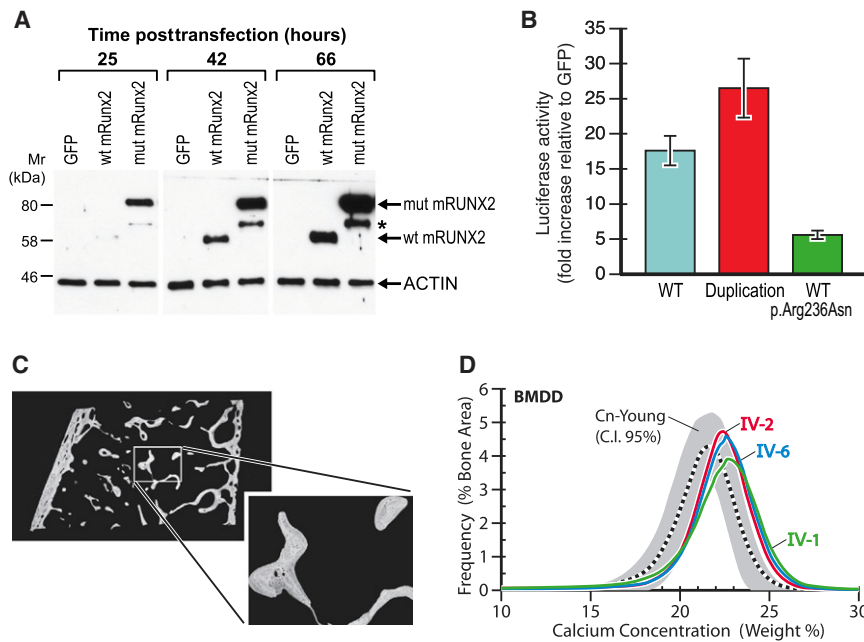


Figure 3. Functional Characterization of the Intragenic *RUNX2* Duplication

(A) Immunoblot analysis of mouse *RUNX2* proteins (m*RUNX2*) overexpressed in HEK293 cells. Cells were transfected with equal amounts of expression plasmids encoding green fluorescent protein (GFP), wild-type mouse *RUNX2* (wt m*RUNX2*), or mutant mouse *RUNX2* (mut m*RUNX2*) carrying a duplication of exons 3 to 5. At the indicated time points after transfection, total cellular extracts were prepared and analyzed by immunoblotting. The asterisk points to an undetermined minor immunoreactive protein that appears only in lanes containing mutant m*RUNX2*. The blot was rehybridized for actin as a loading control. *RUNX2* protein levels are much higher for the mutated than for the wild-type protein at all three time points.

(B) Relative activity of the mouse -1.1 kb osteocalcin promoter-luciferase reporter construct 42 hr after cotransfection with 300 ng of plasmids encoding the wild-type mouse *RUNX2*, the mutant mouse

RUNX2, or the wild-type mouse *RUNX2* harboring a missense mutation (p.Arg236Asn, corresponding to a p.Arg229Asn change in human *RUNX2*). Data represent means \pm SD from three independent experiments and are expressed as fold induction relative to the GFP control. The duplication in *RUNX2* leads to higher transactivation activity, whereas the p.Arg236Asn mutation is associated with lower transactivation activity.

(C) Backscattered electron image of iliac bone sample from subject IV-1.

(D) Results of bone mineralization density distribution analysis in trabecular bone from subjects IV-1, IV-2, and IV-6, compared to age-matched reference data in cancellous bone (Cn-Young).²² In all three samples the distribution curve is shifted toward higher mineralization density compared to control values.

followed by 17 alanine residues. The runt domain is the functionally essential DNA binding domain of *RUNX2*.⁸

The duplication of exons 3 to 5 was confirmed with cDNA derived from a fibroblast line from subject IV-6. PCR amplification and sequencing by a forward primer in exon 4 and a reverse primer in exon 3 in the subject's cDNA resulted in a PCR product of the predicted length and sequence, confirming that exon 5 was followed by exon 3 and thus proving the forward orientation of the duplication (Figure 2C). This duplication also results in a c.686_687delinsAT (p.Arg229Asn) (NM_001024630.3) change at the breakpoint between exon 5 and exon 3. On the protein level, the duplication of exons 3 to 5 of *RUNX2* thus leads to a p.[Pro21_Arg229dup; Arg229Asn] change. Residue 229 of *RUNX2* is an evolutionary conserved amino acid (Figure S2).

The functional consequences of the duplication in exons 3 to 5 of *RUNX2* were assessed by introducing a similar duplication in murine *Runx2* cDNA. The construct led to the duplication of amino acids 25 to 232 of murine *RUNX2* (corresponding to residues 25 to 225 in human *RUNX2*) and included the Q/A and runt domains, with the exception of the last four amino acids of the runt domain (Figure S2). Equal amounts of expression plasmids containing mutated and wild-type *Runx2* cDNA were transfected into HEK293 cells. The resulting intracellular *RUNX2* proteins migrated at their predicted molecular masses of 57 kDa and 80 kDa, respectively (Figure 3A).

Protein levels were markedly higher for the mutated *RUNX2* than for wild-type *RUNX2*. In addition, we compared the transactivation activity of the mutant to that of the wild-type *RUNX2*, using a reporter construct based on the mouse osteocalcin promoter, which has been well characterized as an osteoblast-specific target of *RUNX2*.⁸ Cotransfection of equal amounts of these constructs in HEK293 cells demonstrated increased transactivation activity for the mutated *RUNX2* (Figure 3B). A separate analysis of the functional effect of the isolated Arg to Asn change at the breakpoint residue 229 showed that this sequence change led to decreased transactivation activity (Figure 3B). Overall, these transfection experiments suggested that the duplication of exons 3 to 5 leads to some loss of transactivation activity of the *RUNX2* protein as a result of the amino acid change at residue 229, but a marked increase in intracellular *RUNX2* protein levels, with the composite effect of a gain in function.

Mice overexpressing *Runx2* in osteoblasts have an abnormally low number of osteocytes in cortical bone.^{9,10} We therefore determined cortical osteocyte density in the iliac bone samples from subjects IV-1, IV-2, and IV-6 and in three age-matched control samples that were taken from our reference collection.¹¹ This revealed that osteocyte density (the number of osteocytes relative to the cortical bone area of the section) was 32% lower in the samples from affected individuals than in controls (mean \pm SE: 186 ± 13 mm⁻² versus 272 ± 4 mm⁻²).

Runx2 transgenic mice have a lower-than-normal average material density of trabecular bone.¹⁰ Therefore, material bone density was also determined in the iliac bone samples from subjects IV-1, IV-2, and IV-6, but in contrast to the mouse studies we found that material density was slightly increased compared to controls (Figure 3C).

In this report we present a kindred in which several members presented with the MDMHB phenotype. Even though the family link to the MDMHB kindred described by Halal et al.¹ could not be ascertained, the family presented here had strikingly similar features and originated from the same geographic area. The main phenotypic difference between the two families is that Halal et al.¹ had reported brachydactyly, whereas acral abnormalities were not observed in the individuals presented here. However, brachydactyly was an inconsistent feature in the family described by Halal et al.¹ Therefore, we consider it very likely that the family described by Halal et al.¹ and the individuals presented here have in fact the same disorder, MDMHB, and may in fact be individuals from the same extended family.

RUNX2 is the master regulator of both osteoblast and terminal chondrocyte differentiation and is essential for in vivo bone formation and mineralization.^{4,12} A large number of bone-related genes are regulated by RUNX2, which binds to DNA and heterodimerizes with the transcriptional coactivator core binding factor b.¹³ Both of these functions are mediated by the runt domain that is duplicated in individuals with MDMHB.¹⁴

Until now, CCD has been the only disorder associated with *RUNX2* mutations. All of the more than 170 *RUNX2* mutations reported until now are believed to result in loss of RUNX2 function and lead to CCD.^{6-8,15} MDMHB affects similar skeletal sites as CCD, but in some ways represents the mirror image of CCD. Clavicles are enlarged in MDMHB but are hypoplastic or absent in CCD. In MDMHB, the cranial vault is thickened whereas there is a lack of skull mineralization in CCD. Persons with MDMHB present with dystrophic teeth, whereas CCD is associated with supernumerary teeth. The MDMHB phenotype is also different from that caused by duplications of the entire *RUNX2* locus, which are associated with susceptibility to premature cranial suture fusion.^{16,17}

The clinical findings of MDMHB and the results of our mechanistic studies are in accordance with the notion that the duplication of exons 3 to 5 leads to a gain of function in RUNX2. This gain of function may result from increased cellular levels of mutated RUNX2 protein, as suggested by our transfection experiments. The mechanism leading to this increase in levels of mutated RUNX2 protein was not investigated in this study, but it is known that RUNX2 levels are regulated by complex posttranslational modifications.¹⁸ One or several of these posttranslational modification pathways may be affected by the duplication. The situation is made even more complicated by the fact that the duplication of exons 3 to 5 in RUNX2 not only leads to the addition of 209 amino acids to the

protein but also introduces an amino acid change at the breakpoint residue 229, which by itself seems to lead to a decrease in transactivation activity of RUNX2. Possibly, the marked increase in the amount of mutated protein overrides this decrease in function.

RUNX2 is an important regulator of osteoblast function, so it may be surprising that the in vivo consequence of this putative gain-of-function mutation was decreased osteoblast activity, as shown by the low mineral apposition rate in bone samples of subjects with MDMHB. A similar discrepancy between in vitro and in vivo effects was found in *Runx2*-overexpressing mice.¹⁹ A possible explanation is that RUNX2 must be suppressed during osteoblast differentiation for immature osteoblasts to become fully mature.^{9,10,20} A gain of RUNX2 function may therefore interfere with osteoblast maturation, which is consistent with our observation that in bone tissue of individuals with MDMHB there are fewer-than-normal osteocytes, the terminal stage of osteoblast maturation. Correspondingly, mice overexpressing *Runx2* in osteoblasts have a severe deficit in bone formation, leading to thin long-bone cortices, low bone mass, and low osteocyte density.^{9,10} Similarly, overexpression of *Runx2* in odontoblasts interferes with the maturation of these cells and leads to disordered tooth structure.²¹ These skeletal and dental features of *Runx2* overexpression in mice were also present in individuals with MDMHB. However, it appears that bones arising through intramembranous bone formation (skull, clavicle) do not follow the same pattern; indeed, the radiographic appearance of clavicles and skull suggests that the amount of bone is increased at these locations.

The effect of *Runx2* overexpression on bone resorption is somewhat inconsistent between mouse models; both normal and markedly elevated bone resorption have been reported.^{9,10} In subjects with MDMHB, there was no indication of increased bone resorption and bone turnover seemed to be somewhat low. This is consistent with the finding that material bone density was slightly elevated in the bone samples from these individuals. Lower bone turnover means that the average time since bone deposition at a given skeletal location is higher, allowing more time to complete bone matrix mineralization.

In summary, this report shows that MDMHD is caused by a duplication in *RUNX2* that may lead to a gain-of-function and a bone formation defect, thus enlarging the phenotypic spectrum associated with dysregulation of RUNX2 function.

Supplemental Data

Supplemental Data include two figures and four tables and can be found with this article online at <http://www.cell.com/AJHG/>.

Acknowledgments

We are indebted to Rose Travers and Guy Charette for bone sample processing and histomorphometric analyses; to Patty Mason and

Marie-Hélène Gaumond for assistance with functional studies; and to Mark Lepik for preparing the figures. We would like to thank Janet Marcadier (Clinical Coordinator) for her contribution to the infrastructure of the FORGE Canada Consortium. FORGE Canada Consortium (Finding of Rare Disease Genes in Canada) Steering Committee: Kym Boycott (leader; University of Ottawa), Jan Friedman (colead; University of British Columbia), Jacques Michaud (colead; Université de Montréal), Francois Bernier (University of Calgary), Michael Brudno (University of Toronto), Bridget Fernandez (Memorial University), Bartha Knoppers (McGill University), Mark Samuels (Université de Montréal), and Steve Scherer (University of Toronto). The authors wish to acknowledge the contribution of The Centre for Applied Genomics (Toronto, Canada) for performing the microarray studies and the McGill University and Génome Québec Innovation Centre (Montreal, Canada) for performing the exome sequencing.

This work was supported by the Shriners of North America and received funding by the Government of Canada through Genome Canada, the Canadian Institutes of Health Research, and the Ontario Genomics Institute (OGI-049). Additional funding was provided by Genome Quebec, Genome British Columbia, and the McLaughlin Centre. F.R. received support from the Chercheur-Boursier Clinicien program of the Fonds de recherche du Québec - Santé.

Received: August 24, 2012

Revised: November 21, 2012

Accepted: December 3, 2012

Published: January 3, 2013

Web Resources

The URLs for data presented herein are as follows:

DGV, Genomic Variants in Human Genome, http://dgvbeta.tcag.ca/gb2/gbrowse/dgv2_hg19/

Human Gene Mutation Database, <http://www.hgmd.org/>

Online Mendelian Inheritance in Man (OMIM), <http://www.omim.org/>

RefSeq, <http://www.ncbi.nlm.nih.gov/RefSeq>

UCSC Genome Browser, <http://genome.ucsc.edu>

References

- Halal, F., Picard, J.L., Raymond-Tremblay, D., and de Bosset, P. (1982). Metaphyseal dysplasia with maxillary hypoplasia and brachydactyly. *Am. J. Med. Genet.* *13*, 71–79.
- Abecasis, G.R., Cherny, S.S., Cookson, W.O., and Cardon, L.R. (2002). Merlin—rapid analysis of dense genetic maps using sparse gene flow trees. *Nat. Genet.* *30*, 97–101.
- Schwartzentruber, J., Korshunov, A., Liu, X.Y., Jones, D.T., Pfaff, E., Jacob, K., Sturm, D., Fontebasso, A.M., Quang, D.A., Tönjes, M., et al. (2012). Driver mutations in histone H3.3 and chromatin remodelling genes in paediatric glioblastoma. *Nature* *482*, 226–231.
- Otto, F., Thornell, A.P., Crompton, T., Denzel, A., Gilmour, K.C., Rosewell, I.R., Stamp, G.W., Beddington, R.S., Mundlos, S., Olsen, B.R., et al. (1997). *Cbfa1*, a candidate gene for cleidocranial dysplasia syndrome, is essential for osteoblast differentiation and bone development. *Cell* *89*, 765–771.
- Long, F. (2012). Building strong bones: molecular regulation of the osteoblast lineage. *Nat. Rev. Mol. Cell Biol.* *13*, 27–38.
- Mundlos, S., Otto, F., Mundlos, C., Mulliken, J.B., Aylsworth, A.S., Albright, S., Lindhout, D., Cole, W.G., Henn, W., Knoll, J.H., et al. (1997). Mutations involving the transcription factor *CBFA1* cause cleidocranial dysplasia. *Cell* *89*, 773–779.
- Ott, C.E., Leschik, G., Trotier, F., Brueton, L., Brunner, H.G., Brussel, W., Guillen-Navarro, E., Haase, C., Kohlhase, J., Kotzot, D., et al. (2010). Deletions of the *RUNX2* gene are present in about 10% of individuals with cleidocranial dysplasia. *Hum. Mutat.* *31*, E1587–E1593.
- Yoshida, T., Kanegane, H., Osato, M., Yanagida, M., Miyawaki, T., Ito, Y., and Shigesada, K. (2002). Functional analysis of *RUNX2* mutations in Japanese patients with cleidocranial dysplasia demonstrates novel genotype-phenotype correlations. *Am. J. Hum. Genet.* *71*, 724–738.
- Liu, W., Toyosawa, S., Furuichi, T., Kanatani, N., Yoshida, C., Liu, Y., Himeno, M., Narai, S., Yamaguchi, A., and Komori, T. (2001). Overexpression of *Cbfa1* in osteoblasts inhibits osteoblast maturation and causes osteopenia with multiple fractures. *J. Cell Biol.* *155*, 157–166.
- Geoffroy, V., Kneissel, M., Fournier, B., Boyde, A., and Mathias, P. (2002). High bone resorption in adult aging transgenic mice overexpressing *cbfa1/runx2* in cells of the osteoblastic lineage. *Mol. Cell. Biol.* *22*, 6222–6233.
- Glorieux, F.H., Travers, R., Taylor, A., Bowen, J.R., Rauch, F., Norman, M., and Parfitt, A.M. (2000). Normative data for iliac bone histomorphometry in growing children. *Bone* *26*, 103–109.
- Komori, T., Yagi, H., Nomura, S., Yamaguchi, A., Sasaki, K., Deguchi, K., Shimizu, Y., Bronson, R.T., Gao, Y.H., Inada, M., et al. (1997). Targeted disruption of *Cbfa1* results in a complete lack of bone formation owing to maturational arrest of osteoblasts. *Cell* *89*, 755–764.
- Komori, T. (2011). Signaling networks in *RUNX2*-dependent bone development. *J. Cell. Biochem.* *112*, 750–755.
- Kagoshima, H., Shigesada, K., Satake, M., Ito, Y., Miyoshi, H., Ohki, M., Pepling, M., and Gergen, P. (1993). The Runt domain identifies a new family of heteromeric transcriptional regulators. *Trends Genet.* *9*, 338–341.
- Hansen, L., Riis, A.K., Silahtaroglu, A., Hove, H., Lauridsen, E., Eiberg, H., and Kreiborg, S. (2011). *RUNX2* analysis of Danish cleidocranial dysplasia families. *Clin. Genet.* *79*, 254–263.
- Wilkie, A.O., Bochukova, E.G., Hansen, R.M., Taylor, I.B., Rannan-Eliya, S.V., Byren, J.C., Wall, S.A., Ramos, L., Venâncio, M., Hurst, J.A., et al. (2007). Clinical dividends from the molecular genetic diagnosis of craniosynostosis. *Am. J. Med. Genet. A.* *143A*, 1941–1949.
- Mefford, H.C., Shafer, N., Antonacci, F., Tsai, J.M., Park, S.S., Hing, A.V., Rieder, M.J., Smyth, M.D., Speltz, M.L., Eichler, E.E., and Cunningham, M.L. (2010). Copy number variation analysis in single-suture craniosynostosis: multiple rare variants including *RUNX2* duplication in two cousins with metopic craniosynostosis. *Am. J. Med. Genet. A.* *152A*, 2203–2210.
- Jonason, J.H., Xiao, G., Zhang, M., Xing, L., and Chen, D. (2009). Post-translational regulation of *Runx2* in bone and cartilage. *J. Dent. Res.* *88*, 693–703.
- He, N., Xiao, Z., Yin, T., Stubbs, J., Li, L., and Quarles, L.D. (2011). Inducible expression of *Runx2* results in multiorgan abnormalities in mice. *J. Cell. Biochem.* *112*, 653–665.
- Maruyama, Z., Yoshida, C.A., Furuichi, T., Amizuka, N., Ito, M., Fukuyama, R., Miyazaki, T., Kitaura, H., Nakamura, K.,

- Fujita, T., et al. (2007). Runx2 determines bone maturity and turnover rate in postnatal bone development and is involved in bone loss in estrogen deficiency. *Dev. Dyn.* *236*, 1876–1890.
21. Li, S., Kong, H., Yao, N., Yu, Q., Wang, P., Lin, Y., Wang, J., Kuang, R., Zhao, X., Xu, J., et al. (2011). The role of runt-related transcription factor 2 (Runx2) in the late stage of odontoblast differentiation and dentin formation. *Biochem. Biophys. Res. Commun.* *410*, 698–704.
22. Fratzl-Zelman, N., Roschger, P., Misof, B.M., Pfeffer, S., Glorieux, F.H., Klaushofer, K., and Rauch, F. (2009). Normative data on mineralization density distribution in iliac bone biopsies of children, adolescents and young adults. *Bone* *44*, 1043–1048.

Supplemental Data

Metaphyseal Dysplasia with Maxillary Hypoplasia and Brachydactyly Is Caused

by a Duplication in *RUNX2*

Pierre Moffatt, Mouna Ben Amor, Francis H. Glorieux, Paul Roschger, Klaus Klaushofer, Jeremy A. Schwartzentruber, Andrew D. Paterson, Pingzhao Hu, Christian Marshall, FORGE Canada Consortium, Somayyeh Fahiminiya, Jacek Majewski, Chandree L. Beaulieu, Kym M. Boycott, and Frank Rauch

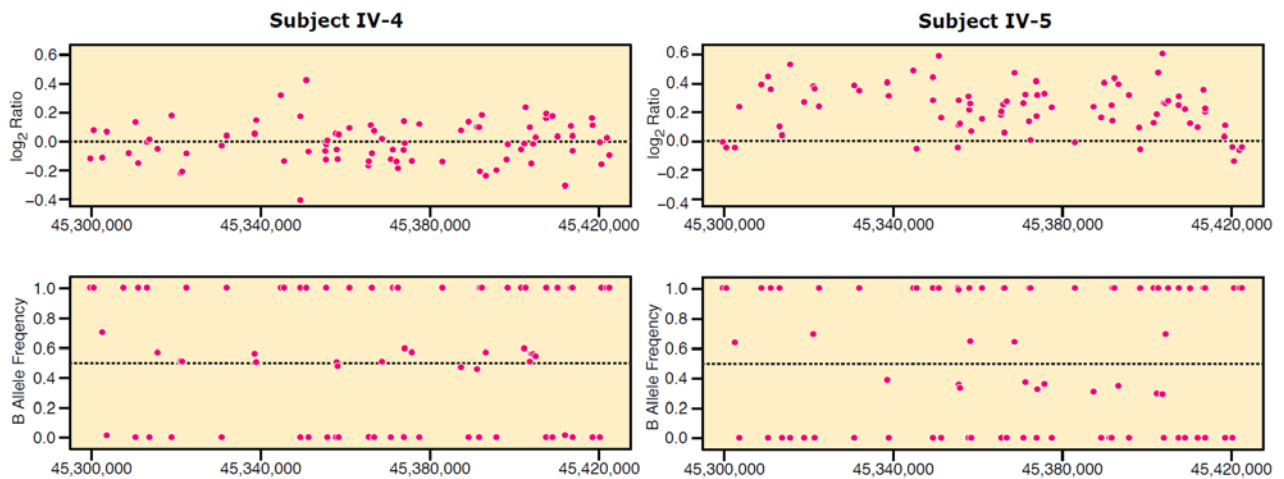


Figure S1. Copy Number Variation Analysis of SNP Array Data. LogR intensity (upper panels) and B allele frequency plots (lower panels) from unaffected subject IV-4 and his affected sister, subject IV-5, are shown as examples.

			1	50
hum	RUNX2	(1)	MASNSLFS	TVTPCQQNFFWDPSTSRRFSPSSSLQPGKMSDVSPVVAQQ
mus	RUNX2	(1)	MASNSLFS	AVTPCQQSFFWDPSTSRRFSPSSSLQPGKMSDVSPVVAQQ
			51	100
hum	RUNX2	(51)	QQQQQQQQQQQQQQQQQQQQQQQ	-----E-AAAAAAAAAAAAAAAAAAVPRL
mus	RUNX2	(51)	QQQQQQQQQQQQQQQQQQQQQQQ	FAAAAAAAAAAAAAAAAAAAVPRL
			101	150
hum	RUNX2	(94)	RPPHDNRTMVEIIADHPAELVRTDSPNFLCSVLP	SHWRCNKTLPVAFKVV
mus	RUNX2	(101)	RPPHDNRTMVEIIADHPAELVRTDSPNFLCSVLP	SHWRCNKTLPVAFKVV
			151	200
hum	RUNX2	(144)	ALGEVPDGTVVTVMAGNDENYSAELRNASAVMKNQVARFNDLRFVGRSGR	
mus	RUNX2	(151)	ALGEVPDGTVVTVMAGNDENYSAELRNASAVMKNQVARFNDLRFVGRSGR	
			201	250
hum	RUNX2	(194)	GKSFTLTITVFTNPPQVATYHRAIKVTVDGPREPR	HRQKLDDSKPSLFS
mus	RUNX2	(201)	GKSFTLTITVFTNPPQVATYHRAIKVTVDGPREPR	HRQKLDDSKPSLFS
			251	300
hum	RUNX2	(244)	DRLSDLGRIPHPSMRVGVPPQNPRPSLNSAPSPFNPQGQSQITDPRQAQS	
mus	RUNX2	(251)	DRLSDLGRIPHPSMRVGVPPQNPRPSLNSAPSPFNPQGQSQITDPRQAQS	
			301	350
hum	RUNX2	(294)	SPPWSYDQSYPSYLSQMTSPSIHSTTPLSSTRGTGLPAITDVPRI	SDDD
mus	RUNX2	(301)	SPPWSYDQSYPSYLSQMTSPSIHSTTPLSSTRGTGLPAITDVPRI	SDDD
			351	400
hum	RUNX2	(344)	TATSDFLWPS	TLSKKSQAGASELGPFSDPRQFPSISL
mus	RUNX2	(351)	TATSDFLWPS	SLSKKSQAGASELGPFSDPRQFPSISL
			401	450
hum	RUNX2	(394)	YPATFTYTPPVTSGMSLGMSATTHYHTYLPPYPGSSQSQSGPFQTSSTP	
mus	RUNX2	(401)	YPATFTYTPPVTSGMSLGMSATTHYHTYLPPYPGSSQSQSGPFQTSSTP	
			451	500
hum	RUNX2	(444)	YLYYGTSS	GSYQFPMVPGGDRSPSRMLPPCTTTSNGSTLLNP
mus	RUNX2	(451)	YLYYGTSS	ASVQFPMVPGGDRSPSRMLPPCTTTSNGSTLLNP
			501	528
hum	RUNX2	(494)	VDADGSHSSSPTVLNSSGRMDES	VWRPY
mus	RUNX2	(501)	VDADGSHSSSPTVLNSSGRMDES	VWRPY

Figure S2. Amino Acid Sequence of Human and Mouse RUNX2. Amino acids affected by the duplication of exons 3 to 5 in human *RUNX2* are highlighted by yellow background. The breakpoint residue at position 229 (position 236 in the mouse sequence) is indicated by turquoise background. The amino acids affected by the duplication generated in a construct of murine *Runx2* cDNA that was used for functional studies are shown with green background. Amino acid differences between human and mouse RUNX2 are shown in black letters and white background.

Table S1. Clinical Characteristics of MDMHB

	III-2	III-3	IV-1	IV-2	IV-5	IV-6
Sex	F	F	F	F	F	F
Age at first visit (years)	50	41	16	14	15	17
Final height (cm)	152 (<P5)	159 (P10)	161 (P25)	153 (<P5)	146 (<P5)	155 (P5)
Bone pain	None	None	Back pain	None	Knee++	Back+++
Extremity fractures	None		Shoulder at 10 y	Tibia 2x; 5th finger; 2nd toe		
Facial features	Maxillary hypoplasia	No abnormalities	Maxillary hypoplasia	Maxillary hypoplasia	Narrow forehead; beaked nose; thin lips; short philtrum; maxillary hypoplasia	Narrow forehead; beaked nose; thin lips; short philtrum; maxillary hypoplasia
Dental status	Dystrophic yellowish teeth	Dystrophic yellowish teeth; abscesses; total dental extraction at 15 y	Dystrophic yellowish teeth	Dystrophic yellowish teeth	Dystrophic yellowish teeth	Dystrophic yellowish teeth; total dental extraction at 21 y

Table S2. Radiographic Findings in MDMHB

	IV-1	IV-2	IV-5	IV-6
Acral anomalies	nd	nd	None	None
Skull	nd	nd	Mild calvarial thickening, closed sutures	Mild calvarial thickening, closed sutures
Clavicles	nd	nd	Enlargement of proximal halves	Enlargement of proximal halves
Spine	Compression fractures	Lumbar lordosis	Mild thoracic compression fractures	Moderate to severe compression fractures
Pelvis	nd	nd	Large ischial branches	Large ischial branches
Long bones	nd	nd	Metaphyseal flare, undertubulation of diaphyses	Metaphyseal flare, undertubulation of diaphyses

Abbreviations: nd: not done

Only spine x-rays were available for subjects III-2 and III-3

Table S3. Biochemical and Bone Densitometric Results in MDMHB

	Norm	III-2	III-3	IV-1	IV-2	IV-5	IV-6
Age (years)		50	41	25	23	21	17
<i>Serum and Urine Biochemistry</i>							
Ionized calcium (mmol/L)	1.19 to 1.32	1.31	1.31	1.26	1.27	1.26	1.23
Inorganic phosphorus (mmol/L)	0.73 to 1.53	1.39	1.48	1.09	1.03	1.27	1.01
Parathyroid hormone (pmol/L)	2.6 to 10	7.5	7.2	9.2	9.8	8.4	9.1
25-hydroxyvitamin D (nmol/L)	50 to 125	57	53	48	82	59	72
Alkaline phosphatase (U/L)	11 to 113	100	77	49	87	47	52
Urinary NTx/creatinine (nmol/mmol)	5 to 64	75	40	21	41	36	88
<i>Lumbar Spine Dual Energy X-Ray Absorptiometry</i>							
Areal BMD (z-score)	-2 to +2	0.2	-0.7	-3.7	-2.9	-0.9	-3.1
<i>Peripheral Quantitative Computed Tomography (Radius Metaphysis, '4% site')</i>							
Total cross sectional area (z-score)	-2 to +2	0.7	nd	2.8	1.0	2.4	1.7
Cortical thickness (z-score)	-2 to +2	-3.7	nd	-5.8	-6.8	-6.3	-2.9
Trabecular volumetric BMD (z-score)	-2 to +2	-1.3	nd	-3.5	-1.9	-1.2	-2.3
<i>Peripheral Quantitative Computed Tomography (Radius Diaphysis, '65% site')</i>							
Total cross sectional area (z-score)	-2 to +2	0.0	nd	1.4	-0.1	1.5	0.8
Cortical thickness (z-score)	-2 to +2	-1.7	nd	-4.2	-3.8	-6.0	-4.8

Abbreviations: nd: not done; BMD: Bone mineral density; NTx: N-telopeptide of collagen type I (a bone resorption marker); nd: not done

Peripheral quantitative computed tomography (XCT-2000, Stratec Inc., Pforzheim, Germany)

was performed as described;^{1;2} z-scores were calculated based on published reference data.^{1;2}

Table S4. Chromosomal Regions with the Maximum Lod Score in SNP Linkage Analysis

Chromosome	LOD	Start Position (hg 19, bp position)	End Position (hg 19, bp position)	Size (Mb)
Chr6	2.1	39,943,696	51,354,544	11.4
Chr11	2.1	12,286,355	16,779,416	4.5
Chr15	2.1	90,219,770	98,025,535	7.8

Supplemental References

1. Rauch, F., and Schoenau, E. (2005). Peripheral quantitative computed tomography of the distal radius in young subjects - new reference data and interpretation of results. *J Musculoskelet Neuronal Interact* 5, 119-126.
2. Rauch, F., and Schoenau, E. (2008). Peripheral quantitative computed tomography of the proximal radius in young subjects - New reference data and interpretation of results. *J Musculoskelet Neuronal Interact* 8, 217-226.